



# Dual topology in van der Waals-type superconductor Nb<sub>2</sub>S<sub>2</sub>C

Xian-Biao Shi<sup>1,2</sup> · Peng He<sup>1,2</sup> · Wei-Wei Zhao<sup>1,2,3</sup>

Received: 24 November 2021 / Revised: 21 December 2021 / Accepted: 21 December 2021 / Published online: 25 February 2022  
© The Nonferrous Metals Society of China 2022

## Abstract

Nb<sub>2</sub>S<sub>2</sub>C is a van der Waals type layered superconductor with a transition temperature  $T_c = 7.6$  K. In this paper, detailed calculations of the electronic structure and topological properties of Nb<sub>2</sub>S<sub>2</sub>C were performed from first principles. We find that Nb<sub>2</sub>S<sub>2</sub>C is a highly anisotropic metal with multi-band characteristics. In the absence of spin–orbit coupling (SOC), there appears one pair of triply degenerate points created by band inversion along the  $\Gamma$ –A line. When SOC is considered, the triple points are gapped. Intriguingly, two distinct types of topological states, including topological Dirac semimetal and topological insulator states, co-emergence in the vicinity of Fermi level. Moreover, the topology of Nb<sub>2</sub>S<sub>2</sub>C is robust to external pressure and the Fermi level can be shifted downward to the topological Dirac semimetal state and topological insulator state at 10 GPa and 14 GPa, respectively. The results herein provide a new platform not only for the studies of physics of low-dimensional superconductor but also for further investigations of topological superconductivity.

**Keywords** Nb<sub>2</sub>S<sub>2</sub>C · Dirac points · Topological insulator · First-principles calculations

## 1 Introduction

Superconductors in van der Waals structure have attracted extensive interest because they provide a new possibility for realizing highly crystalline two-dimensional (2D) superconducting systems with exotic properties that differ from the bulk [1–11]. For instance, atomically thin NbSe<sub>2</sub> crystals have been discovered to host unusual superconducting states, including Ising superconductivity with a strong in-plane upper critical field [3] and a field-induced Bose-metal phase under the out-of-plane magnetic field [4]. Therefore, exploring new quasi-2D superconductors is one of the most

intriguing themes in the field of condensed matter physics [9, 10].

Our title compound, Nb<sub>2</sub>S<sub>2</sub>C, has been already synthesized in 1992 [12] and discovered as a superconductor in 2001 [13]. Below  $T_c = 7.6$  K, Nb<sub>2</sub>S<sub>2</sub>C exhibits type-II bulk superconductivity. Because Nb<sub>2</sub>S<sub>2</sub>C could not be prepared by direct synthesis, its physical properties hence have been scarcely studied [13, 14]. However, its van der Waals type layered structure, endows Nb<sub>2</sub>S<sub>2</sub>C with a promising candidate for realizing a new 2D superconductor. Therefore, investigation on Nb<sub>2</sub>S<sub>2</sub>C in terms of the electronic structure is very valuable.

In this paper, using first-principles calculations, we predict the coexistence of topological Dirac semimetal and topological insulator states in the vicinity of Fermi level ( $E_f$ ) in the bulk electronic band structure of Nb<sub>2</sub>S<sub>2</sub>C. Because the interplay of non-trivial band topology and superconductivity may give rise to topological superconductivity hosting the long pursuing Majorana fermion, which is potential for the use in low decoherence topological quantum computation [15–17], Nb<sub>2</sub>S<sub>2</sub>C as such provides a new platform not only for the studies of physics of 2D superconductor but also for further investigations of topological superconductivity.

✉ Peng He  
hithpeng@hit.edu.cn

✉ Wei-Wei Zhao  
wzhao@hit.edu.cn

<sup>1</sup> State Key Laboratory of Advanced Welding & Joining, Harbin Institute of Technology, Harbin 150001, China

<sup>2</sup> Shenzhen Key Laboratory of Flexible Printed Electronics Technology, Harbin Institute of Technology, Shenzhen 518055, China

<sup>3</sup> Sauvage Laboratory for Smart Materials, The School of Materials Science and Engineering, Harbin Institute of Technology, Shenzhen 518055, China

## 2 Computational methodology

Present first-principles calculations were carried out within the framework of the projector augmented wave (PAW) method [18], and employed the generalized gradient approximation (GGA) with Perdew–Burke–Ernzerhof (PBE) formula [19], as implemented in the Vienna Ab initio Simulation Package (VASP) [20, 21]. The DFT-D2 method was adopted to describe the weak interactions [22]. A kinetic energy cutoff of 500 eV and a  $\Gamma$ -centered  $k$  mesh of  $15 \times 15 \times 7$  were utilized in all calculations. The energy and force difference criterion were defined as  $10^{-6}$  eV and  $0.1 \text{ eV}\cdot\text{nm}^{-1}$  for self-consistent convergence and structural relaxation. The Wannier90 package [23–25] was adopted to construct Wannier functions from the first principles results without an iterative maximal-localization procedure. The WannierTools code [26] was used to investigate the topological features of surface state spectra.

## 3 Results and discussion

The crystal structure of  $\text{Nb}_2\text{S}_2\text{C}$  is shown in Fig. 1a.  $\text{Nb}_2\text{S}_2\text{C}$  occurs in a layered structure described by the hexagonal space group P-3 m1 (No. 164) [12]. It consists of five atomic layers stacked in a sequence of S–Nb–C–Nb–S. The quintuple-layer in bulk  $\text{Nb}_2\text{S}_2\text{C}$  is weakly coupled by van der Waals interaction. The structural parameters of bulk  $\text{Nb}_2\text{S}_2\text{C}$  calculated by PBE and PBE-D2 methods are listed in Table 1 and compared with experimental data. It can be seen from Table 1 that the optimized lattice constants are in reasonable agreement with experimental values when the van der Waals interaction is considered by the PBE-D2 method. In contrast, the PBE method significantly overestimates the lattice parameter constant  $c$ , implying an importance of the van der Waals interaction in  $\text{Nb}_2\text{S}_2\text{C}$ . Table 1 also shows that the

**Table 1** Calculated structural parameters  $a$ ,  $c$  and  $d$  (the thickness of the  $\text{Nb}_2\text{S}_2\text{C}$  layer, as defined in Fig. 1a) using different methods for  $\text{Nb}_2\text{S}_2\text{C}$

	PBE	PBE-D2	Experiment
$a$ (nm)	0.3282	0.3279	0.3268
$c$ (nm)	0.9131	0.8642	0.8547
$d$ (nm)	0.5650	0.5635	0.5744

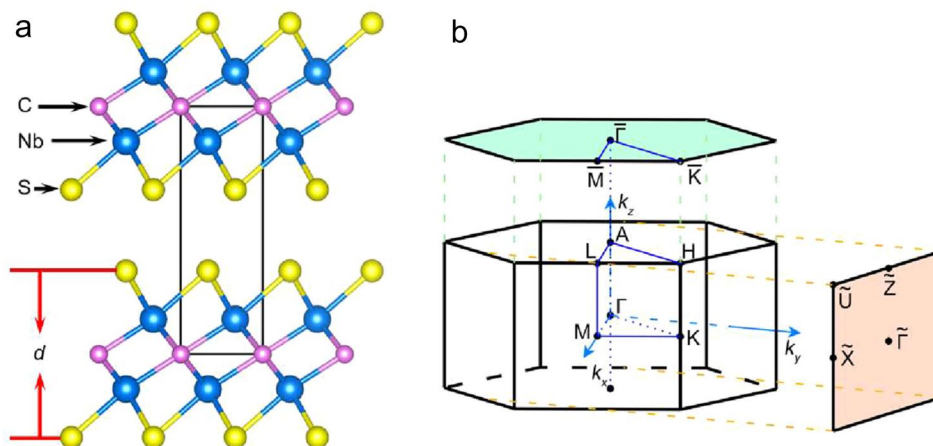
Available experimental values are listed for comparison

effect of the van der Waals interaction is negligible on the thickness of the  $\text{Nb}_2\text{S}_2\text{C}$  layer. We use the lattice parameters optimized by PBE-D2 method in the following calculations. Figure 1b shows the bulk Brillouin zone (BZ), projected (001) and (010) surface BZ, and high symmetry points.

The calculated electronic density of states (DOS) along with atomic projected DOS, plotted in Fig. 2a, shows finite DOS at the  $E_f$ , thus revealing metallic behavior for  $\text{Nb}_2\text{S}_2\text{C}$ . The Nb-4d and S-3p orbitals are widely distributed over all energies below and above the  $E_f$  and dominate the low-energy states of  $\text{Nb}_2\text{S}_2\text{C}$ . The C-2p derived states primarily lie 3.5 eV below the  $E_f$ . Since the DOS at the  $E_f$  has contributions largely from Nb-4d and S-3p states, we thus can emphasize that Nb-4d and S-3p electrons are most efficient in developing the superconducting properties of  $\text{Nb}_2\text{S}_2\text{C}$ .

Figure 2b shows the DFT result of the electronic band structure in the absence of SOC. There are three bands crossing the  $E_f$ , indicating a feature of multi-band superconductivity. The dominant feature of the band is that it shows highly anisotropic dispersion, as expected. The band is highly dispersive along with the in-plane directions, whereas its dispersion is quite small along the out-of-plane direction. The large difference in the dispersions indicates a quasi 2D character of this superconducting system. Intriguingly, there is a triply degenerate band crossing point energy at 0.15 eV below the  $E_f$  along the  $\Gamma$ –A

**Fig. 1** **a** Crystal structure of  $\text{Nb}_2\text{S}_2\text{C}$  from side view. The unit cell is indicated by black contours. **b** Bulk BZ, (001) and (010) projected surface BZ and high symmetry points



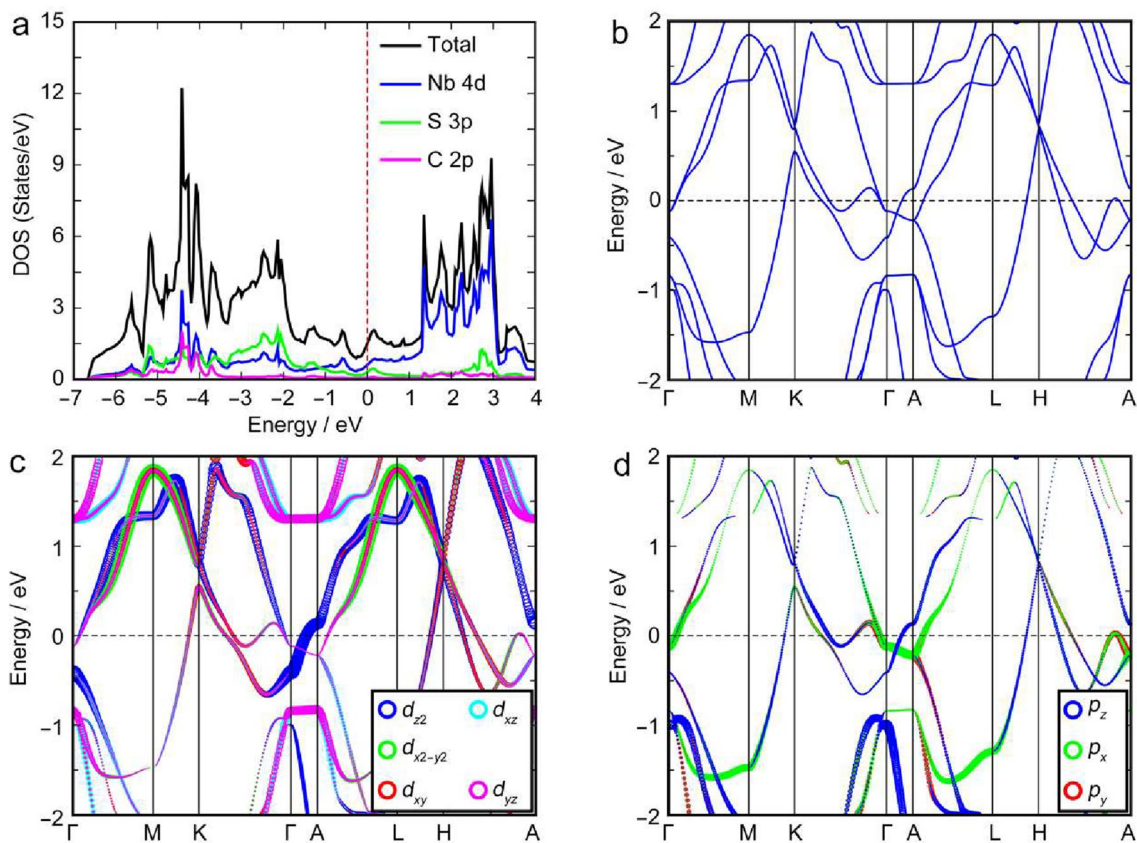


**Fig. 2** **a** Total and projected density of states with specific atomic orbitals. **b** Electronic band structure of Nb<sub>2</sub>S<sub>2</sub>C obtained in the absence of SOC. **c** Band structure projected onto 4d orbitals of Nb atoms. **d** Band structure projected onto 3p orbitals of S atoms

direction. This crossing point is formed by one doubly degenerate band and one nondegenerate band. The orbital projected band structures presented in Fig. 2c, d reveal that the doubly degenerate band is predominantly attributed

to Si-3 $p_{xy}$  orbitals and the nondegenerate band is mainly contributed by Nb-4 $d_{z^2}$  states.

We next calculated the band structure of Nb<sub>2</sub>S<sub>2</sub>C in the presence of SOC, as shown in Fig. 3a. The inclusion of SOC

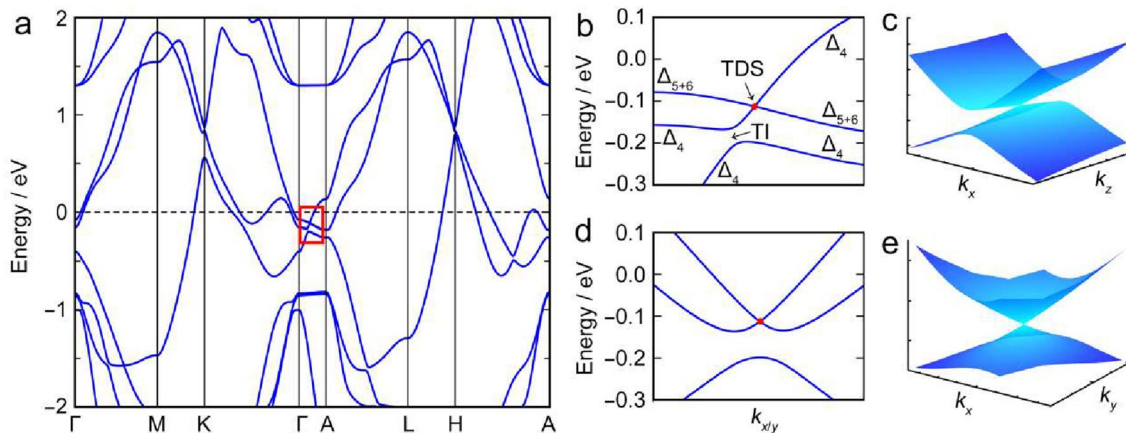


**Fig. 3** **a** Electronic band structure of Nb<sub>2</sub>S<sub>2</sub>C with considering SOC. **b** Enlarged view of the solid red area in **a**. **c** Two-dimensional band structure around the Dirac node in  $k_x$ - $k_z$  plane. **d** Electronic band

structure in  $k_x$ - $k_y$  plane surrounding the Dirac point. **e** Two-dimensional band structure around the Dirac node in  $k_x$ - $k_y$  plane

does not have a significant effect on the overall band dispersions. It does effect on the band crossing point along the  $\Gamma$ -A direction. Upon including SOC, the original triple point is broken. Figure 3b shows the enlarged view of the band structure near the  $E_f$  along the  $\Gamma$ -A direction. There still exists a band crossing point formed by two bands with different irreducible representations ( $\Delta_4$  and  $\Delta_{5+6}$ ). Because of the coexistence of inversion and time-reversal symmetries, all the bands are doubly degenerate [27]. This crossing point as such is fourfold degenerate. Because the  $\Gamma$ -A direction preserves the  $C_3$  rotational symmetry, this crossing point is symmetry protected against hybridization [28]. Around this crossing point, the related bands display linear dispersion along both in-plane and out-of-plane directions, as shown in Figs. 3c, e. Therefore, this crossing point is Dirac point. According to our calculations, there exists a pair of symmetry-protected Dirac points located at BZ coordinates  $(0, 0, k_z^D \approx \pm 0.199 \times \frac{2\pi}{c})$  and energy  $E_D - E_f = -0.113$  eV. In addition to Dirac states, SOC also induces hybridization between two  $\Delta_4$  bands and opens a gap of about 30 meV, leading to topological insulator (TI) states in the  $\Gamma$ -A line, see in Fig. 3b. Because SOC creates a band gap between the two  $\Delta_4$  bands at each  $k$  point, we thus can define a  $Z_2$  invariant by assuming a curved Fermi level between the two  $\Delta_4$  bands to characterize the band topology of  $\text{Nb}_2\text{S}_2\text{C}$ . Using the Wilson loop method [29], we calculate the topological invariant  $Z_2$ . The Wannier charge center (WCC) evolution on the time-reversal invariant planes of  $\text{Nb}_2\text{S}_2\text{C}$  is shown in

Fig. 4, from which we find  $Z_2 = (1; 001)$ , indicating the non-triviality of the band gap.

Exotic topological surface states are an important property to identify various topological phases [30, 31]. Figure 5 shows the calculated surface states on the (001) and (010) projected surfaces. On the (001) surface, a pair of bulk Dirac points on the  $k_z$  axis are projected onto the same  $\bar{\Gamma}$  point, as indicated by the red dot in Fig. 5a. Topological surface states (denoted as SS1) originating from the projection of bulk Dirac points are clearly observed in the inset of Fig. 5a. In addition, a Dirac-cone surface state (denoted as SS2) appears inside the topological insulator gap. For the (010) surface, the pair of bulk Dirac points are projected onto the  $\bar{\Gamma} - \bar{Z}$  surface direction, as indicated by the red dot in Fig. 5b. A surface Dirac cone at the  $\bar{\Gamma}$  point is observed, which is a signal of nontrivial band topology. This surface Dirac cone has its branches merging into the bulk states at the projection of three-dimensional (3D) Dirac point. It should be noted that this surface Dirac cone is distinct to the SS2 on the (001) surface, even though both of them disperse in the same energy range of  $-0.2$  to  $-0.1$  eV. This is because the surface state configuration depends on the details of the surface termination. These surface states obtained on both (001) and (010) surfaces are expected to be observed by angle-resolved photoemission spectroscopy (ARPES).

Considering that the van der Waals type crystal structure of  $\text{Nb}_2\text{S}_2\text{C}$ , external pressure is expected to be an effective and clean way to modulate its electronic structure. To showcase the effect of external pressure on the electronic

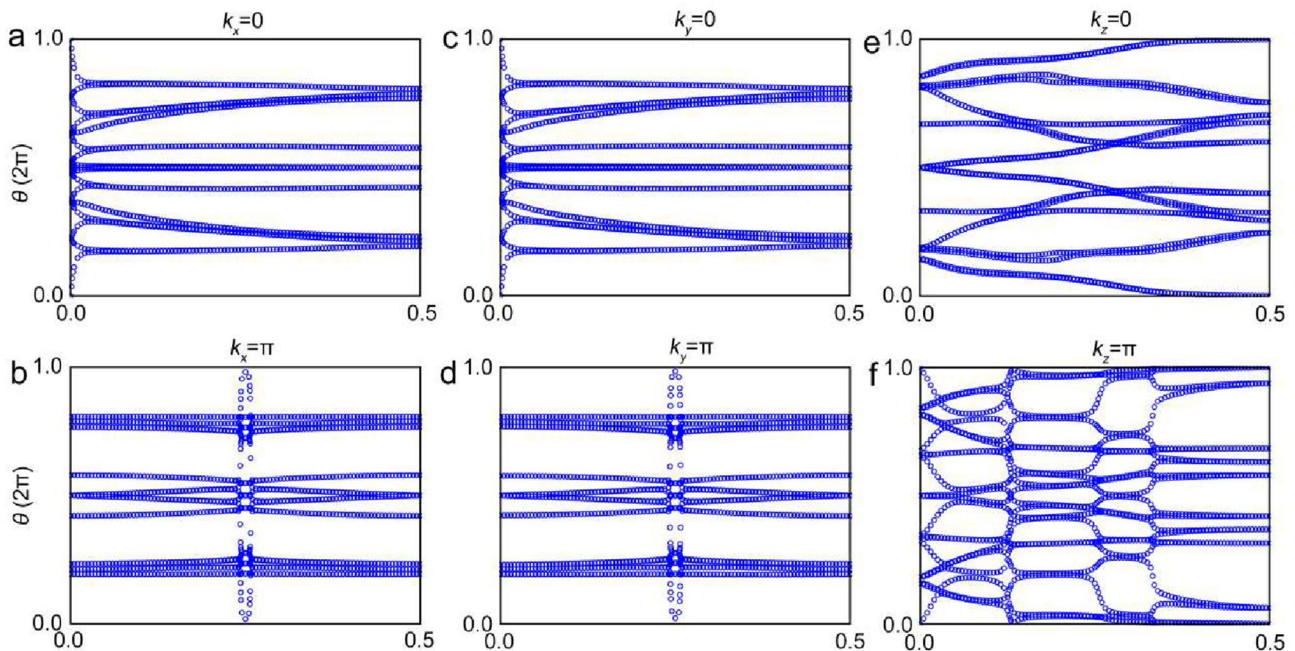


**Fig. 4**  $Z_2$  topological invariants for  $\text{Nb}_2\text{S}_2\text{C}$ . Evolution of Wannier charge centers for **a**  $k_x=0$ , **b**  $k_x=\pi$ , **c**  $k_y=0$ , **d**  $k_y=\pi$ , **e**  $k_z=0$ , and **f**  $k_z=\pi$  time-reversal invariant momentum planes

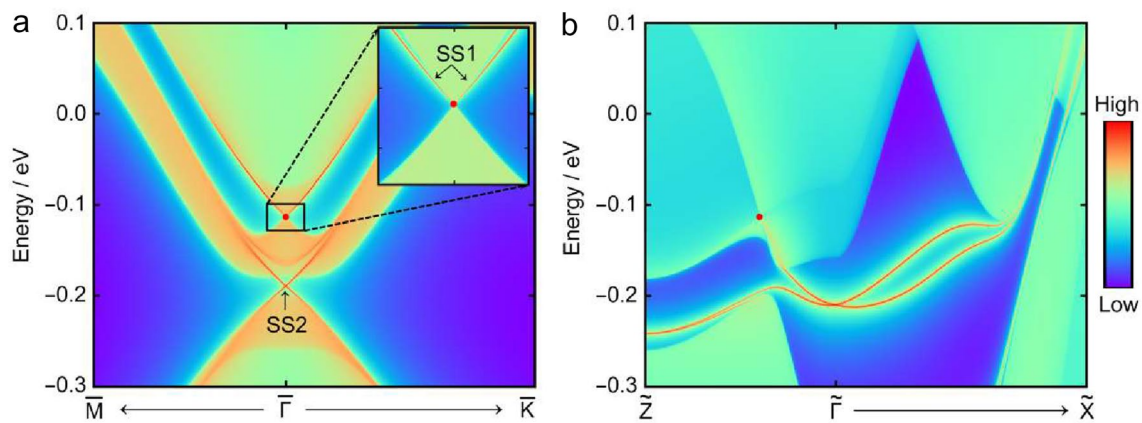


**Fig. 5** Projected surface states of Nb<sub>2</sub>S<sub>2</sub>C for **a** (001) and **b** (010) surfaces. The projected Dirac points are denoted by red dots. The inset shows in **a** the zoom-in view of the solid black box area, where the topological surface states are pointed out by arrows and clearly visible

structure of Nb<sub>2</sub>S<sub>2</sub>C, we carried out calculations of Nb<sub>2</sub>S<sub>2</sub>C under hydrostatic pressure. In Fig. 6a, b, we present our calculated lattice constants as a function of hydrostatic pressure. Lattice parameters *a* and *c* both gradually decrease with the increasing pressure, as expected. Figure 6d, e presents the band structures of Nb<sub>2</sub>S<sub>2</sub>C at 10 GPa and 14 GPa,

respectively. Compared with the band structure at ambient pressure (Fig. 6c), we find that the electron Fermi pockets around the  $\Gamma$  point and along the  $\Gamma$ -K ( $\Gamma$ -K') line disappear when applied pressure larger than 10 GPa, as indicated by the black arrows. Importantly, the bulk Dirac points can be shifted upward to the  $E_f$  at 10 GPa. Increasing pressure up

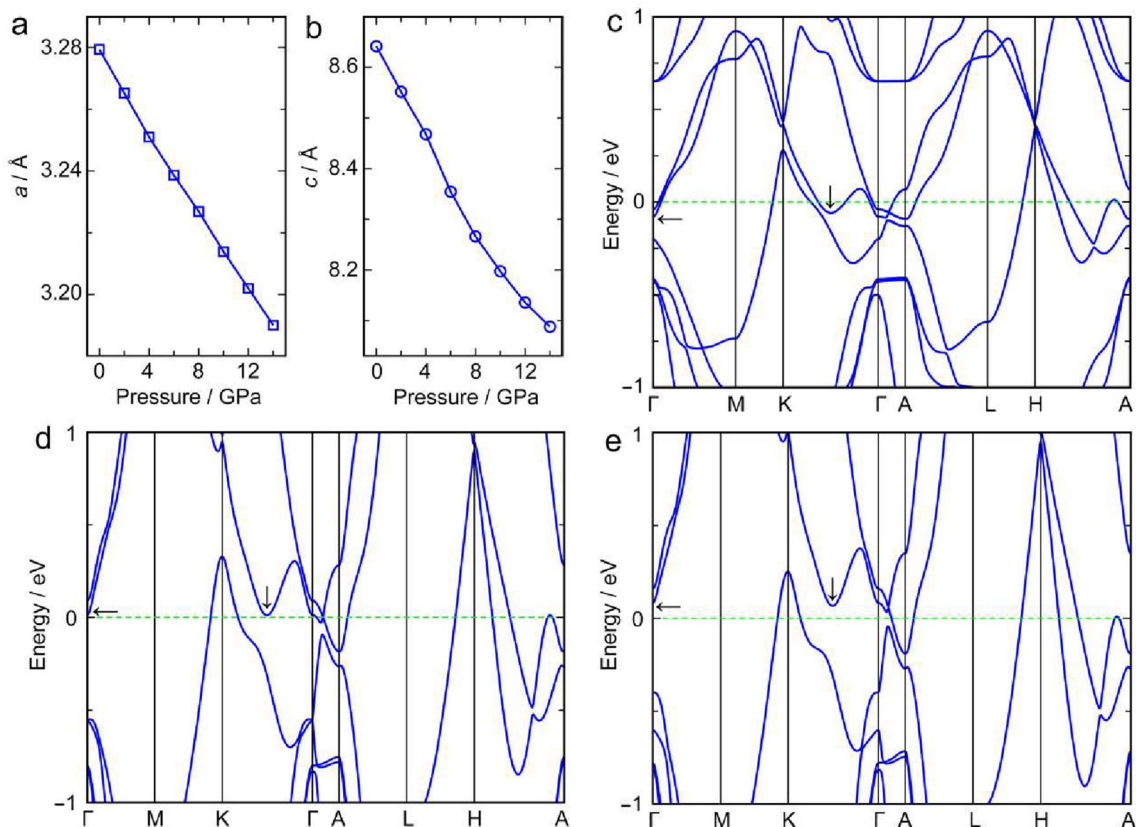


**Fig. 6** Pressure dependencies of lattice parameters **a** and **b** *c*. Electronic band structure of Nb<sub>2</sub>S<sub>2</sub>C with considering SOC at **c** 0 GPa, **d** 10 GPa, and **e** 14 GPa

to 14 GPa, the  $E_f$  is lowered into the bulk topological insulator gap. Therefore, it will be interesting to study the effect of pressure on the superconducting behavior and transport properties of  $\text{Nb}_2\text{S}_2\text{C}$ .

## 4 Conclusion

In conclusion, we have presented the results of first-principles calculations on electronic structure and topological properties for superconductor  $\text{Nb}_2\text{S}_2\text{C}$ . We predict that  $\text{Nb}_2\text{S}_2\text{C}$  is a topological metal hosting topological Dirac semimetal and topological insulator states. The Dirac points are derived from band inversion and protected by  $C_3$  rotational symmetry. The nontrivial surface states are obtained on both (001) and (010) surfaces. Further calculations of external pressure effects suggest the topology of  $\text{Nb}_2\text{S}_2\text{C}$  is robust to external pressure. Interestingly,  $\text{Nb}_2\text{S}_2\text{C}$  has a van der Waals-type layered structure, it thus provides a new platform to experimentally explore low dimensional superconductor and the interactions between superconductivity and multiple nontrivial topological states.

**Acknowledgements** This work was supported by the Natural Science Foundation of China (Grant No. 52073075), Shenzhen Science and Technology Program (Grant No. KQTD20170809110344233), and Science and Technology Innovation Talents Program of Henan Province (Grant No. 174200510010).

## Declarations

**Conflict of interest** The authors declare no conflict of interest.

## References

- Saito Y, Nojima T, Iwasa Y. Highly crystalline 2D superconductors. *Nat Rev Mater*. 2017;2:16094.
- Xi X, Zhao L, Wang Z, Berger H, Forró L, Shan J, Mak FK. Strongly enhanced charge-density wave order in monolayer  $\text{NbSe}_2$ . *Nat Nanotechnol*. 2015;10:765.
- Xi X, Wang Z, Zhao W, Park JH, Law KT, Berger H, Forró L, Shan J, Mak KF. Ising pairing in superconducting  $\text{NbSe}_2$  atomic layers. *Nat Phys*. 2016;12:139.
- Tsen AW, Hunt B, Kim YD, Yuan ZJ, Jia S, Cava RJ, Hone J, Kim P, Dean CR, Pasupathy AN. Nature of the quantum metal in a two-dimensional crystalline superconductor. *Nat Phys*. 2016;12:208.
- Arguilla MQ, Katoch J, Krymowski K, Krymowski ND, Xu J, Xi X, Hanks A, Jiang S, Ross RD, Koch RJ, Ulstrup S, Bostwick A, Jozwiak C, McComb DW, Rotenberg E, Shan J, Windl W, Kawakami RK, Goldberger JE.  $\text{NaSn}_2\text{As}_2$ : an exfoliable layered van der Waals zintl phase. *ACS Nano*. 2016;10:9500.
- Goto Y, Yamada A, Matsuda TD, Aoki Y, Mizuguchi Y. SnAs-based layered superconductor  $\text{NaSn}_2\text{As}_2$ . *J Phys Soc Jpn*. 2017;86:123701.
- Kim JS. A new van der Waals type superconductor. *JPSJ News Comments*. 2017;14:13.
- Ishihara K, Takenaka T, Miao Y, Tanaka O, Mizukami Y, Usui H, Kuroki K, Konczykowski M, Goto Y, Mizuguchi Y, Shibauchi T. Evidence for s-wave pairing with atomic scale disorder in the van der Waals superconductor  $\text{NaSn}_2\text{As}_2$ . *Phys Rev B*. 2018;98:020503(R).
- Cheng EJ, Ni JM, Meng FQ, Ying TP, Pan BL, Huang YY, Peets DC, Zhang QH, Li SY. Nodeless superconductivity in the SnAs-based van der Waals-type superconductor  $\text{NaSn}_2\text{As}_2$ . *Europhys Lett*. 2018;123:47004.
- Li YL, Stavrou E, Zhu Q, Clarke SM, Li Y, Huang HM. Superconductivity in the van der Waals Layered Compound  $\text{PS}_2$ . *Phys Rev B*. 2019;99:220503(R).
- Parvin F, Naqib SH. Pressure dependence of structural, elastic, electronic, thermodynamic, and optical properties of van der Waals-type  $\text{NaSn}_2\text{P}_2$  pnictide superconductor: Insights from DFT study. *Results Phys*. 2021;21:103848.
- Boller H, Hiebl K. Quaternary pseudo-intercalation phases  $\text{Tx} [\text{Nb}_2\text{S}_2\text{C}]$  ( $T \equiv \text{V, Cr, Mn, Fe Co, Ni, Cu}$ ) and metastable  $\text{Nb}_2\text{S}_2\text{C}$  formed by topochemical synthesis. *J Alloys Compd*. 1992;183:438.
- Sakamaki K, Wada H, Nozaki H, Onuki Y, Kawai M. van der Waals type carbosulfide superconductor. *Solid State Commun*. 2001;118:113.
- Sakamaki K, Wada H, Nozaki H, Onuki Y, Kawai M. Topochemical formation of van der Waals type niobium carbosulfide  $1\text{T-Nb}_2\text{S}_2\text{C}$ . *J Alloys Compd*. 2002;339:283.
- Xia W, Shi X, Zhang Y, Su H, Wang Q, Ding L, Chen L, Wang X, Zou Z, Yu N, Pi L, Hao Y, Li B, Zhu Z, Zhao W, Kou X, Guo Y. Bulk Fermi surface of the layered superconductor  $\text{TaSe}_3$  with three-dimensional strong topological state. *Phys Rev B*. 2020;101:155117.
- Zhang G, Shi X, Liu X, Xia W, Su H, Chen L, Wang X, Yu N, Zou Z, Zhao W, Guo Y. de Haas-van Alphen quantum oscillations in  $\text{BaSn}_3$  superconductor with multiple Dirac fermions. *Chin Phys Lett*. 2020;37:087101.
- Huang Z, Shi X, Zhang G, Liu Z, Cho S, Jiang Z, Liu Z, Liu J, Yang Y, Xia W, Zhao W, Guo Y, Shen D. Photoemission spectroscopic evidence of multiple Dirac cones in superconducting  $\text{BaSn}_3$ . *Chin Phys Lett*. 2021;38:107403.
- Blöchl PE. Projector augmented-wave method. *Phys Rev B*. 1994;50:17953.
- Perdew JP, Burke K, Ernzerhof M. Generalized gradient approximation made simple. *Phys Rev Lett*. 1996;77:3865.
- Kresse G, Hafner J. Ab initio molecular-dynamics simulation of the liquid-metal-amorphous semiconductor transition in germanium. *Phys Rev B*. 1994;49:14251.
- Kresse G, Furthmüller J. Efficient iterative schemes for *ab initio* total-energy calculations using a plane-wave basis set. *Phys Rev B*. 1996;54:11169.
- Grimme S. Semiempirical GGA-type density functional constructed with a long-range dispersion correction. *J Comput Chem*. 2006;27:1787.
- Mostofi AA, Yates JR, Lee Y-S, Souza I, Vanderbilt D, Marzari N. wannier90: a tool for obtaining maximally-localised Wannier functions. *Comput Phys Commun*. 2008;178:685.
- Marzari N, Vanderbilt D. Maximally localized generalized Wannier functions for composite energy bands. *Phys Rev B*. 1997;56:12847.
- Souza I, Marzari N, Vanderbilt D. Maximally localized Wannier functions for entangled energy bands. *Phys Rev B*. 2001;65:035109.
- Wu QS, Zhang SN, Song HF, Troyer M, Soluyanov AA. WannierTools: an open-source software package for novel topological materials. *Comput Phys Commun*. 2018;224:405.

27. Weng H, Liang Y, Xu Q, Yu R, Fang Z, Dai X, Kawazoe Y. Topological node-line semimetal in three-dimensional graphene networks. *Phys Rev B*. 2015;92:045108.
28. Yang BJ, Nagaosa N. Classification of stable three-dimensional Dirac semimetals with nontrivial topology. *Nat Commun*. 2014;5:4898.
29. Yu R, Qi XL, Bernevig A, Fang Z, Dai X. Equivalent expression of  $Z_2$  topological invariant for band insulators using the non-Abelian Berry connection. *Phys Rev B*. 2011;84:075119.
30. Wang Z, Sun Y, Chen X-Q, Franchini C, Xu G, Weng H, Dai X, Fang Z. Dirac semimetal and topological phase transitions in  $A_3\text{Bi}$  ( $A = \text{Na, K, Rb}$ ). *Phys Rev B*. 2012;85:195320.
31. Wang Z, Weng H, Wu Q, Dai X, Fang Z. Three-dimensional Dirac semimetal and quantum transport in  $\text{Cd}_3\text{As}_2$ . *Phys Rev B*. 2013;88:125427.

**Publisher's Note** Springer Nature remains neutral with regard to jurisdictional claims in published maps and institutional affiliations.